LEAP-Asia-2018 Numerical Simulation Exercise

Zhijian Qiu

Graduate Student Researcher, UC San Diego

Ahmed Elgamal

Professor of Geotechnical Engineering, UC San Diego

Department of Structural Engineering

University of California, San Diego

La Jolla, California 92093-0085

February 8th 2019

CONTENT

FIGURES

1. Brief Summary of Experiments

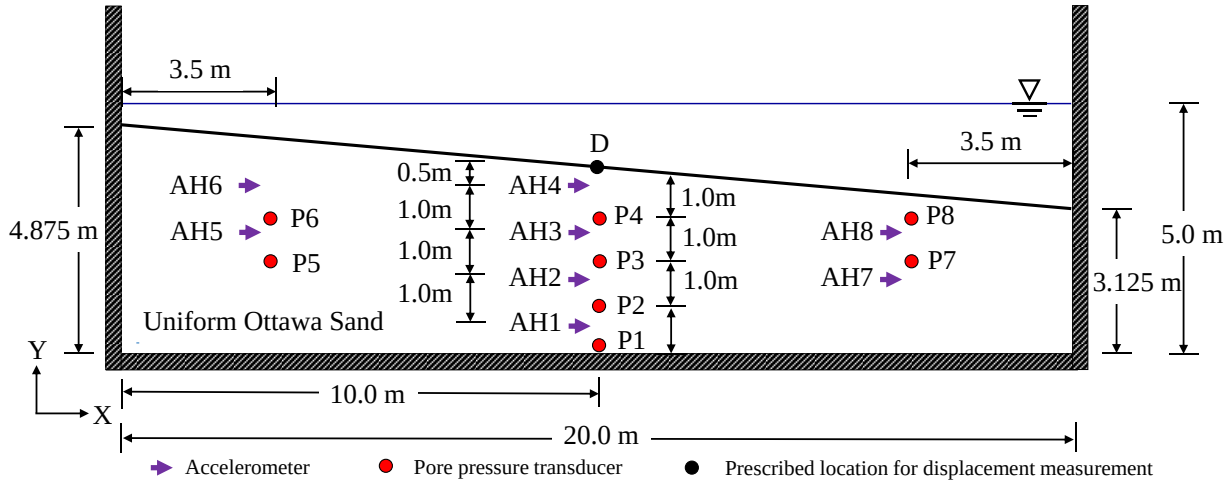

Figure 1. Schematic representation of the centrifuge test layout.

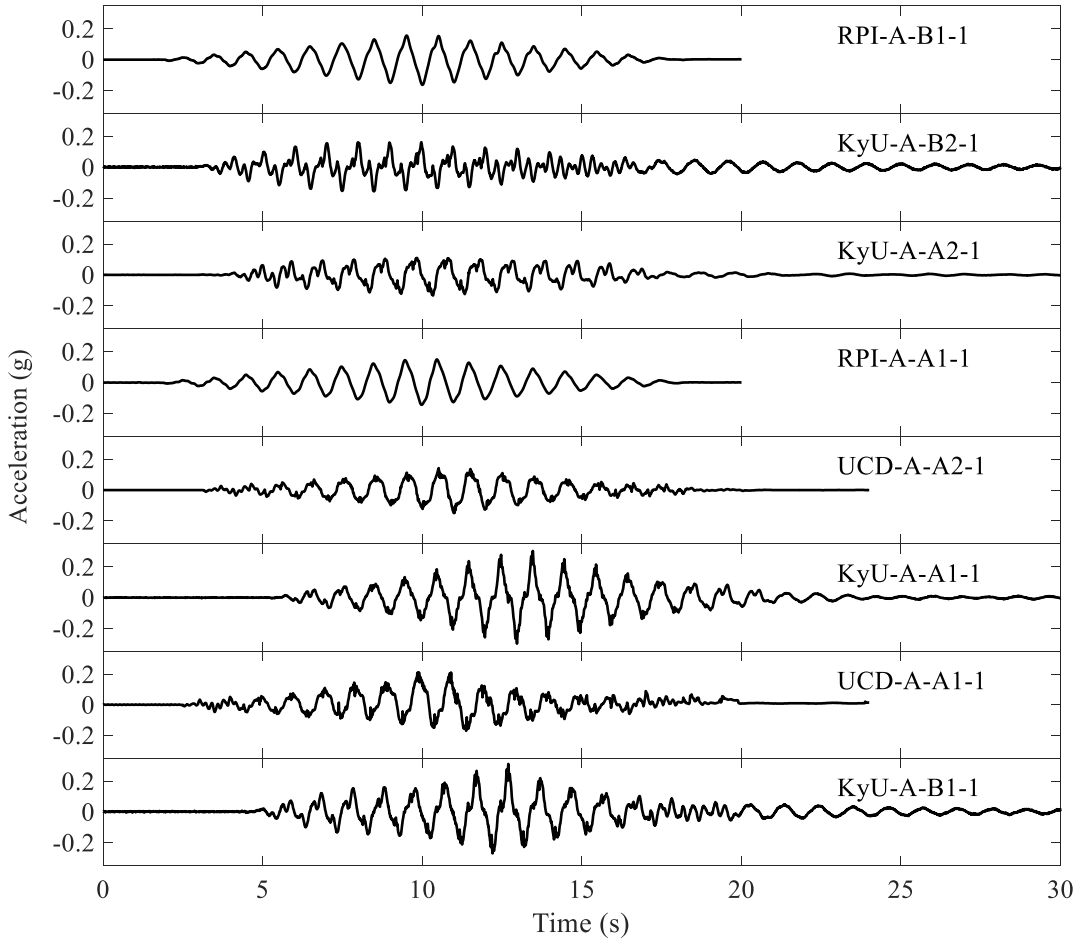

Figure 2. Input motions for LEAP-ASIA-2018 simulations.

Table 1: Summary of centrifuge experiments selected for LEAP-ASIA-2018.

	Density (kg/m^3)	Dr (%)
RPI-A-B1-1	1644	62
KyU-A-B2-1	1633	58
KyU-A-A2-1	1628	56
RPI-A-A1-1	1651	64
UCD-A-A2-1	1658	67
*KyU-A-A1-1	1677	73
*UCD-A-A1-1	1713	86
*KyU-A-B1-1	1673	72

* Optional

2. Finite Element Model

A two-dimensional FE mesh with element size 0.5 m (Fig. 3) is created to represent the centrifuge model with rigid walls. All numerical simulations for the selected 9 centrifuge experiments (Table 1) are conducted using the computational platform OpenSees. The Open System for Earthquake Engineering Simulation (OpenSees, McKenna *et al.* 2010, http://opensees.berkeley.edu) developed by the Pacific Earthquake Engineering Research (PEER) Center, is an open source, object-oriented finite element platform. Currently, OpenSees is widely used for simulation of structural and geotechnical systems (Yang 2000; Yang and Elgamal 2002) under static and seismic loading.

Four-node plane-strain elements with two-phase material following the *u-p* (Chan 1988) formulation were employed for simulating saturated soil response, where *u* is the displacement of the soil skeleton and *p* is the pore water pressure. Implementation of the *u-p* element is based on the following assumptions: 1) small deformation and rotation; 2) solid and fluid density remain constant in time and space; 3) porosity is locally homogeneous and constant with time; 4) soil grains are incompressible; 5) solid and fluid phases are accelerated equally. Hence, the soil layers represented by effective stress fully coupled *u-p* elements are capable of accounting for soil deformations and the associated changes in pore water pressure.

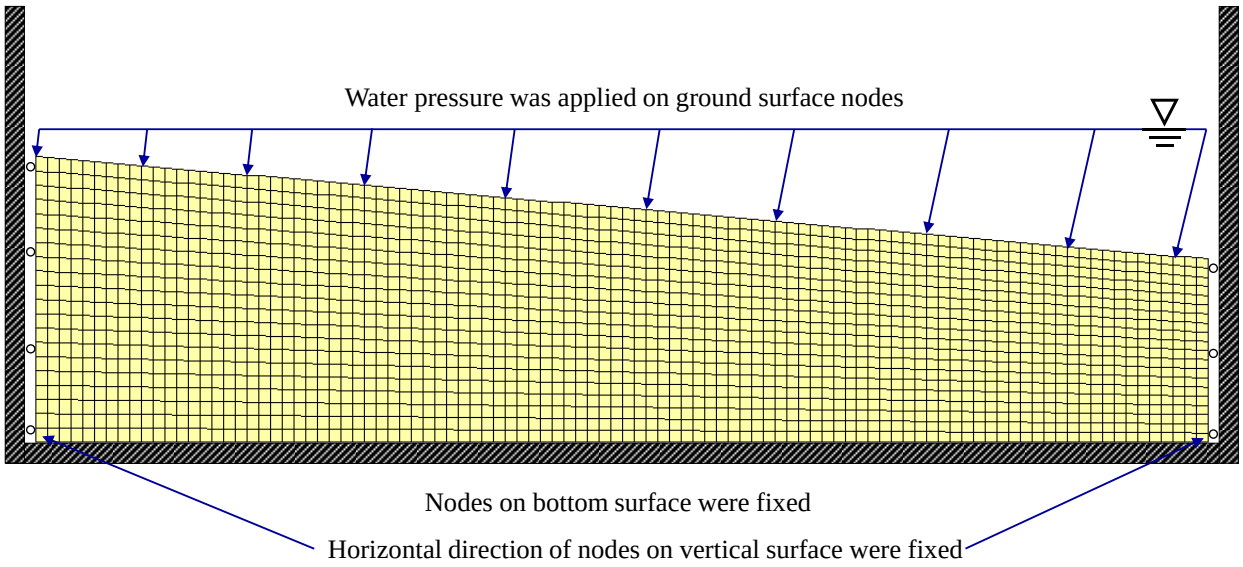

Figure 3. Finite Element mesh (element size = 0.5 m)

3 **Soil constitutive model**

The employed soil constitutive model (Yang 2000; Elgamal *et al.* 2003; Parra 1996; Yang and Elgamal 2002) were developed based on the multi-surface-plasticity theory (Morz 1967; Iwan 1967; Prevost 1978; Prevost 1985). In this employed soil constitutive model, the shear-strain backbone curve was represented by the hyperbolic relationship with the shear strength based on simple shear (reached at an octahedral shear strain of 10%). The small strain shear modulus under a reference effective confining pressure p'_r is computed using the equation $G = G_0(p'/p'_r)^n$, where p' is effective confining pressure. The dependency of shear modulus on confining pressure is taken as (n = 0.5). The critical state frictional constant M_f (failure surface) is related to the friction angle ϕ (Chen and Mizuno 1990) and defined as M_f = 6sinϕ/(3-sinϕ). As such, the soil is simulated by the implemented OpenSees material PressureDependMultiYield02. Brief descriptions of this soil constitutive model are included below.

3.1. Yield function

The yield function is defined as a conical surface in principal stress space (Prevost 1985, Lacy 1986; Yang and Elgamal 2002):

$$f = \frac{3}{2}\left(\boldsymbol{s} - \left(p' + p'_0\right)\boldsymbol{a}\right) : \left(\boldsymbol{s} - \left(p' + p'_0\right)\boldsymbol{a}\right) - M^2\left(p' + p'_0\right)^2 = 0 \qquad (1)$$

where, $\boldsymbol{s} = \boldsymbol{\sigma}' - p'\boldsymbol{\delta}$ is the deviatoric stress tensor, $\boldsymbol{\sigma}'$ is the effective Cauchy stress tensor, $\boldsymbol{\delta}$ is the second-order identity tensor, p' is mean effective stress, p'_0 is a small positive constant (0.3 kPa in this paper) such that the yield surface size remains finite at $p' = 0$ for numerical convenience and to avoid ambiguity in defining the yield surface normal to the yield surface apex. $\boldsymbol{a}$ is a second-order deviatoric tensor defining the yield surface center in deviatoric stress subspace, *M* defines the yield surface size, and ":" denotes doubly contracted tensor product.

3.2. Contractive phase

Shear-induced contraction occurs inside the phase transformation (PT) surface ($\eta < \eta_{PT}$), as well as outside ($\eta > \eta_{PT}$) when $\dot{\eta} < 0$, where, η is the stress ratio and η_{PT} is the stress ratio at phase transformation surface. The contraction flow rule is defined as (Yang *et al.* 2003):

$$P'' = \left(1 - \frac{\dot{\boldsymbol{n}} : \dot{\boldsymbol{s}}}{||\dot{\boldsymbol{s}}||}\frac{\eta}{\eta_{PT}}\right)^2 (c_1 + c_2\gamma_d)\left(\frac{p'}{p_a}\right)^{c_3}(c_4 \times CSR)^{c_5} \qquad (2)$$

where c_1,-c_5 are non-negative calibration constants, γ_d is octahedral shear strain accumulated during previous dilation phases, p_a is atmospheric pressure for normalization purpose, *CSR* is cyclic stress ratio, and $\dot{\boldsymbol{s}}$ is the deviatoric stress rate. The $\dot{\boldsymbol{n}}$ and $\dot{\boldsymbol{s}}$ tensors are used to account for general 3D loading scenarios, where, $\dot{\boldsymbol{n}}$ is the outer normal to a surface. The parameter c_3 is used to represent the dependence of pore pressure buildup on initial confinement (i.e., K_σ effect).

3.3. Dilative phase

Dilation appears only due to shear loading outside the PT surface ($\eta > \eta_{PT}$ with $\dot{\eta} > 0$), and is defined as (Yang *et al.* 2003):

$$P" = (1 - \frac{\dot{\boldsymbol{n}}:\dot{\boldsymbol{s}}}{||\dot{\boldsymbol{s}}||}\frac{\eta}{\eta_{PT}})^2 d_1(\gamma_d)^{d_2}(\frac{p'}{p_a})^{-d_3} \quad (3)$$

where d_1, d_2 and d_3 are non-negative calibration constants, and γ_d is the octahedral shear strain accumulated during all dilation phases in the same direction as long as there is no significant who wrote this load reversal. It should be mentioned that γ_d accumulates even if there are small unload-reload phases, resulting in increasingly stronger dilation tendency and reduced rate of shear strain accumulation.

3.4. Neutral phase

When the stress state approaches the PT surface ($\eta = \eta_{PT}$) from below, a significant amount of permanent shear strain may accumulate prior to dilation, with minimal changes in shear stress and p' (implying $p" = 0$). For simplicity, $P" = 0$ is maintained during this highly yielded phase until a boundary defined in deviatoric strain space is reached, and then dilation begins. This yield domain will enlarge or translate depending on load history (Yang *et al.* 2003).

It should be noted that PressureDependMultiYield02 has been improved with new flow rules in order to better capture contraction and dilation in sands and the model parameters were calibrated with established guidelines on the liquefaction triggering logic, i.e., cyclic stress ratio versus number of equivalent uniform loading cycles in undrained (direct simple shear) DSS loading to cause single-amplitude shear strain of 3% (Khosravifar *et al.* 2017).

4 Boundary and loading conditions

The boundary and loading conditions for the dynamic analysis of the sloping ground under an input motion are implemented in a staged fashion as follows:

1) Gravity was applied to activate the initial static state (Fig. 4) for the sloping ground with: i) linear elastic properties (Poisson's ratio of 0.47), ii) nodes on both side boundaries (vertical faces) of the FE model were fixed against longitudinal translation, iii) nodes were fixed along the base against vertical translation, iv) water table was specified (Fig. 2) with related water pressure and nodal forces specified along ground surface nodes. At the end of this step, the static soil state was imposed and displacements under own-weight application were re-set to zero using the OpenSees command InitialStateAnalysis.

2) Soil properties were switched from elastic to plastic.

3) Nodes were fixed along the base against longitudinal translation.

4) Dynamic analysis is conducted by applying an acceleration time history to the base of the FE model.

The FE matrix equation is integrated in time using a single-step predictor multi-corrector scheme of the Newmark type (Chan 1988; Parra 1996) with integration parameters $\gamma = 0.6$ and $\beta = 0.3025$. The equation is solved using the modified Newton-Raphson method, i.e., Krylov subspace acceleration (Carlson and Miller 1998) for each time step. A relatively low level of stiffness proportional damping (coefficient = 0.003) with the main damping emanating from the soil nonlinear shear stress-strain hysteresis response was used to enhance numerical stability of the liquefiable sloping system. The tolerance criteria used to check the convergence is based on the increment of energy with a tolerance of 10^{-6}.

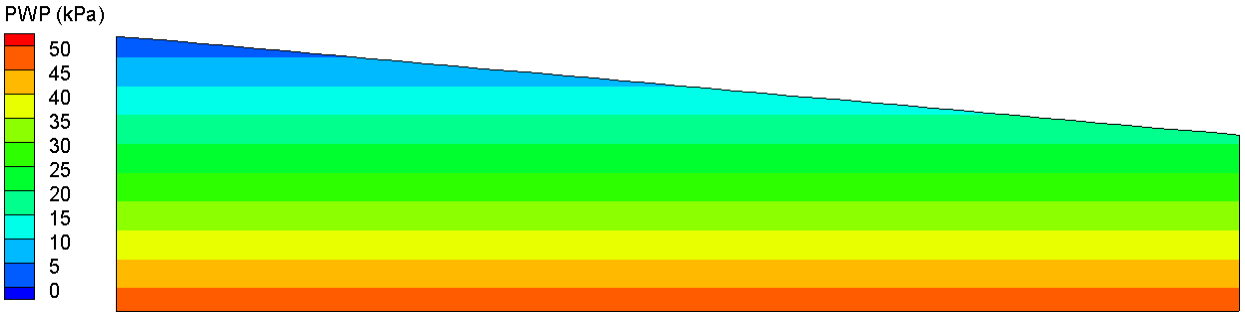

(a)

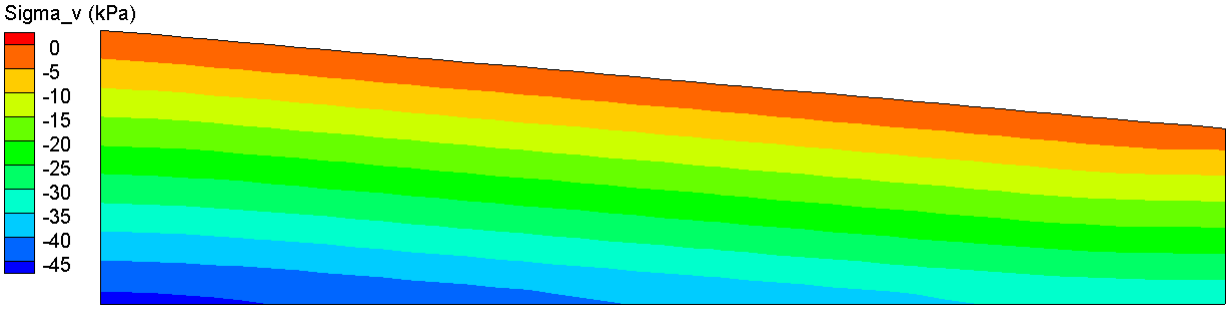

(b)

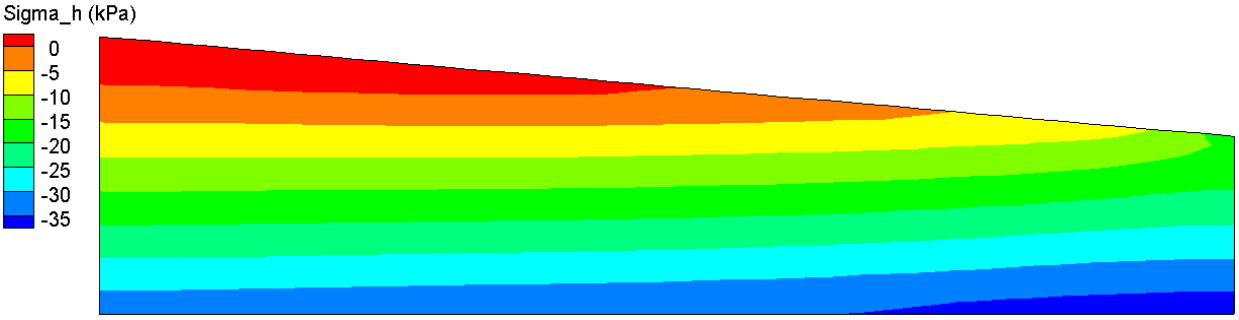

(c)

Figure 4. Initial state of soil due to gravity: (a) Pore water pressure; (b) Vertical stress; (c) Horizontal stress.

5. Determination of Soil Model Parameters for Dr = 60%

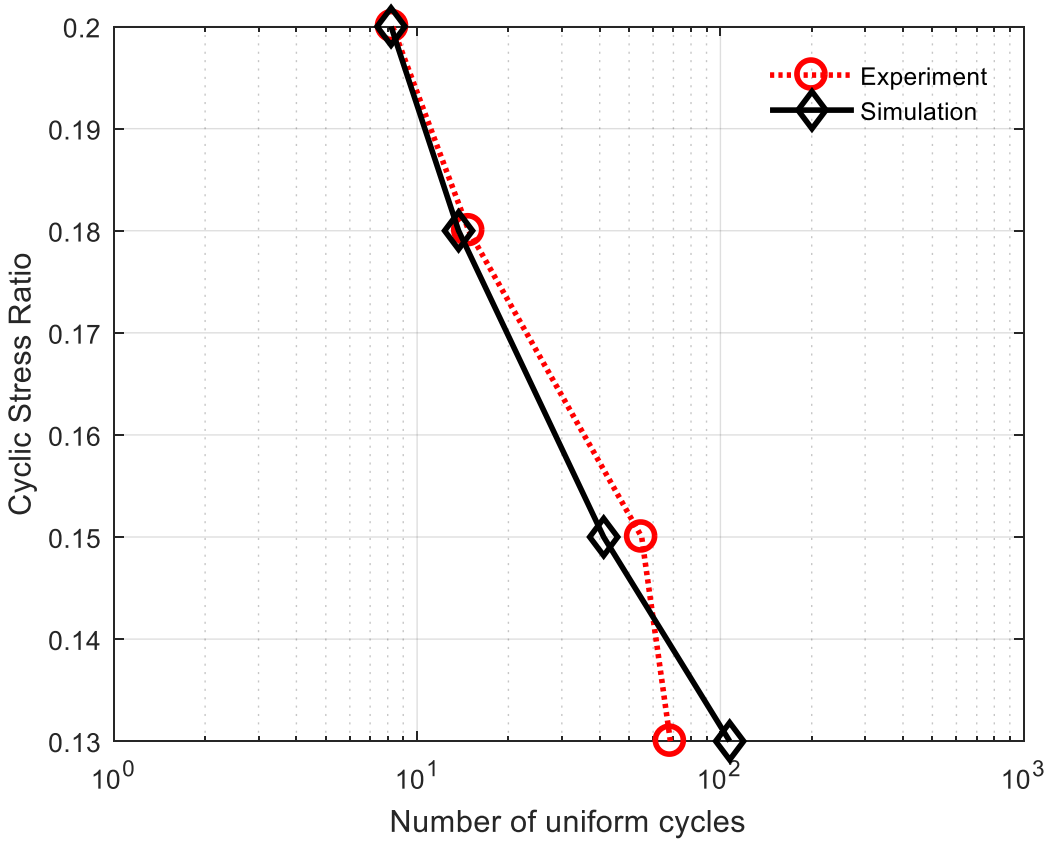

Figure 5. Simulated liquefaction strength curves with measured data for Dr. = 60 %

Table 2: Sand model parameters for Dr = 60%.

Model Parameters	Value
Reference mean effective pressure, p'_r (kPa)	101.0
Mass density ρ (t/m^3)	2.04
Maximum shear strain at reference pressure, $\gamma_{max,r}$	0.1
Shear modulus at reference pressure, G_r (MPa)	25.0
Stiffness dependence coefficient d, $G = G_r(\frac{\boldsymbol{P'}}{\boldsymbol{P'_r}})^{\boldsymbol{d}}$	0.5
Poisson's ratio v (for dynamics)	0.4
Shear strength at zero confinement, c (kPa)	0.3
Friction angle ϕ	44°
Phase transformation angle	36°
Contraction coefficient, c_1	0.028
Contraction coefficient, c_2	5.0
Contraction coefficient, c_3	0.15
Contraction coefficient, c_4	5.5
Contraction coefficient, c_5	4.6
Dilation coefficient, d_1	0.4
Dilation coefficient, d_2	3.0
Dilation coefficient, d_3	0.15
Damage parameter, *Liq1*	0.4
Damage parameter, *Liq2*	3.0
Permeability (m/s)	1.0×10^{-5}
Number of yield surfaces	20

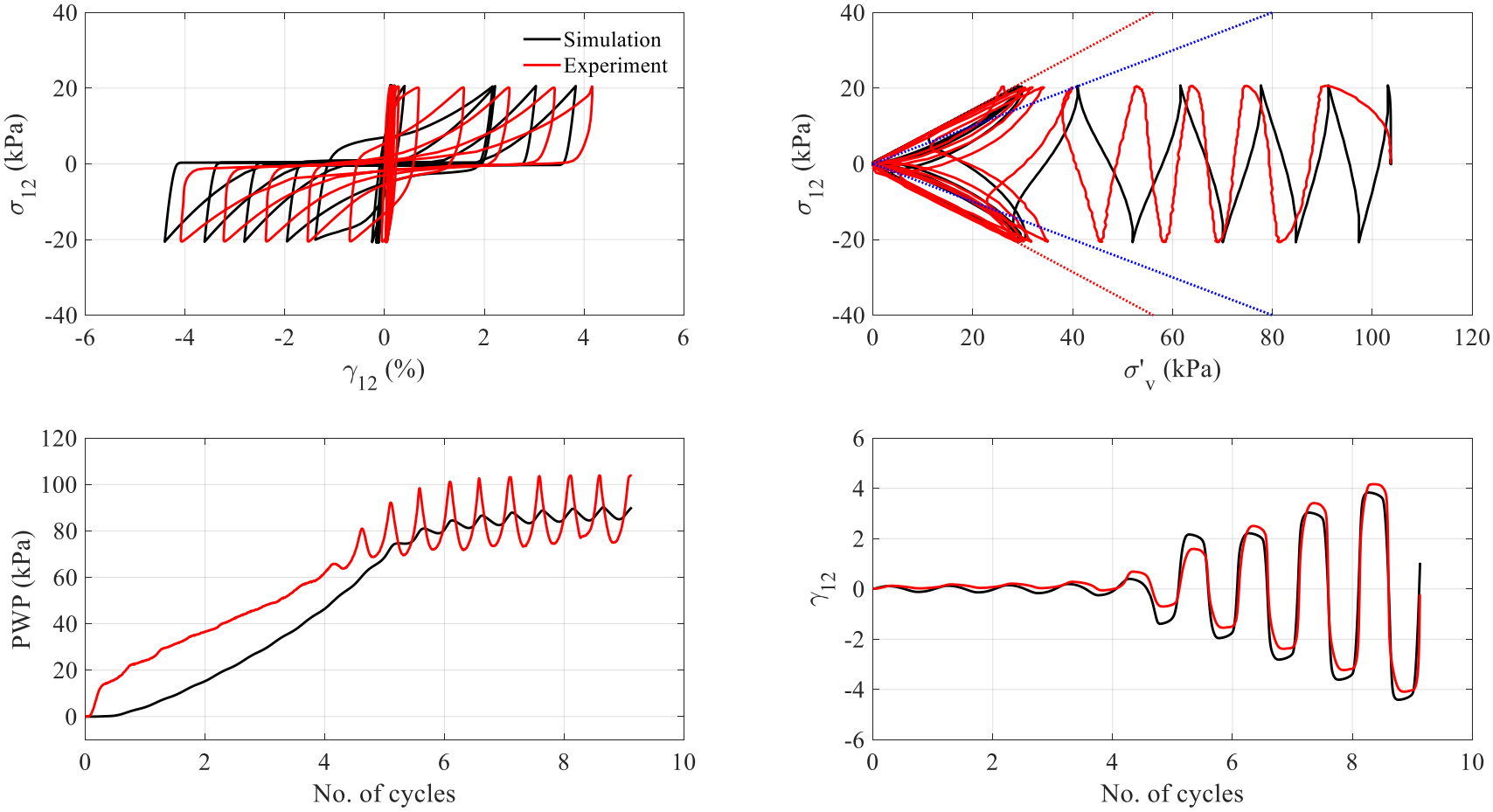

Figure 6. Computed and laboratory results of an isotropically consolidated, undrained monotonic triaxial loading test (Dr = 60%).

6. Computed Results of Type-B Simulations

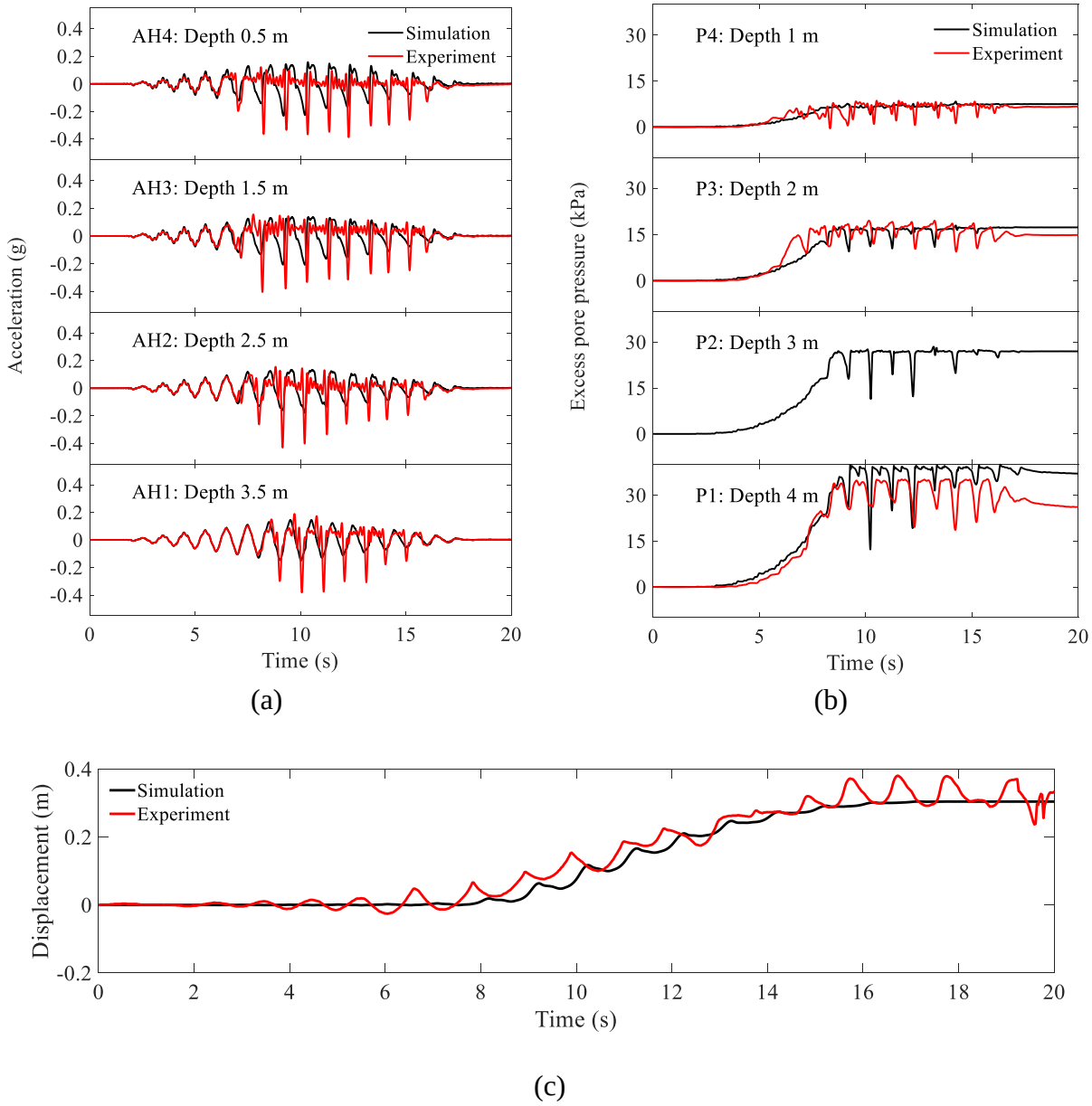

Figure 7. Measured and computed time histories of RPI-A-B1-1: (a) Acceleration; (b) Excess pore water pressure; (c) Displacement at middle of ground surface.

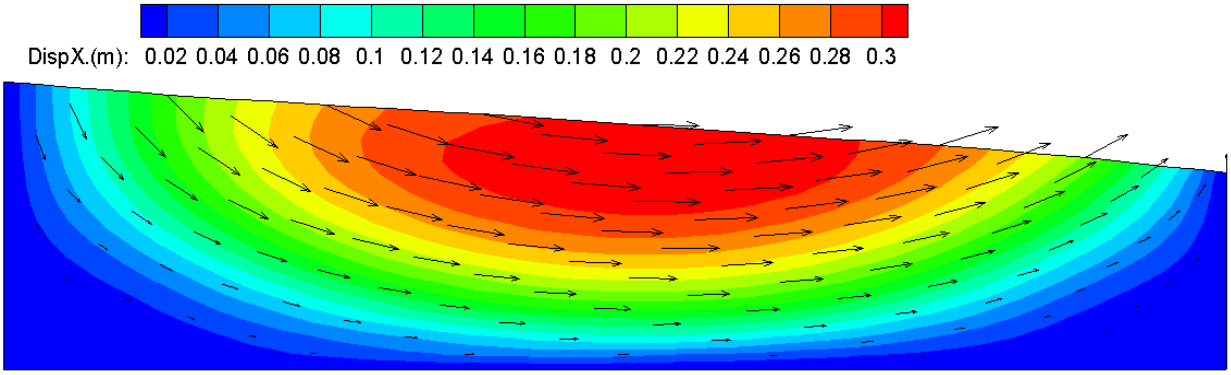

(a)

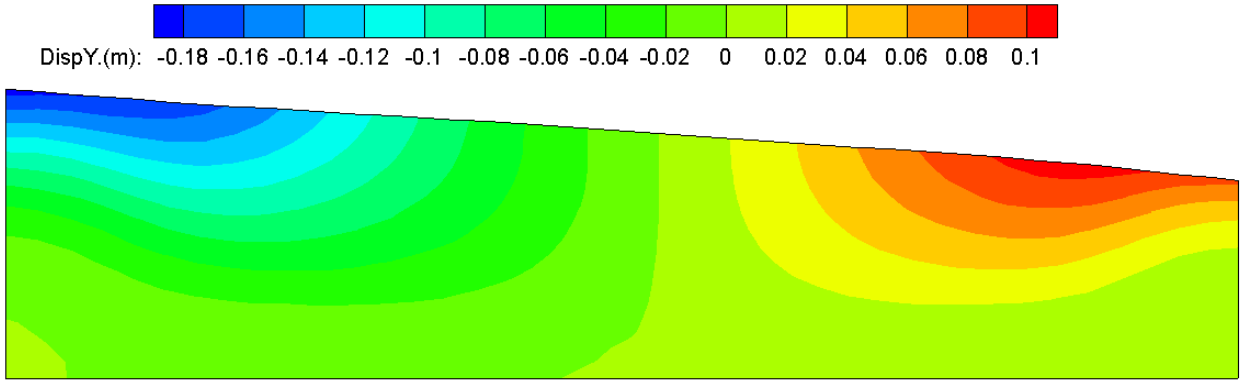

(b)

Figure 8. Computed displacement contours of RPI-A-B1-1: (a) Horizontal (arrow shows the total displacement); (b) Vertical.

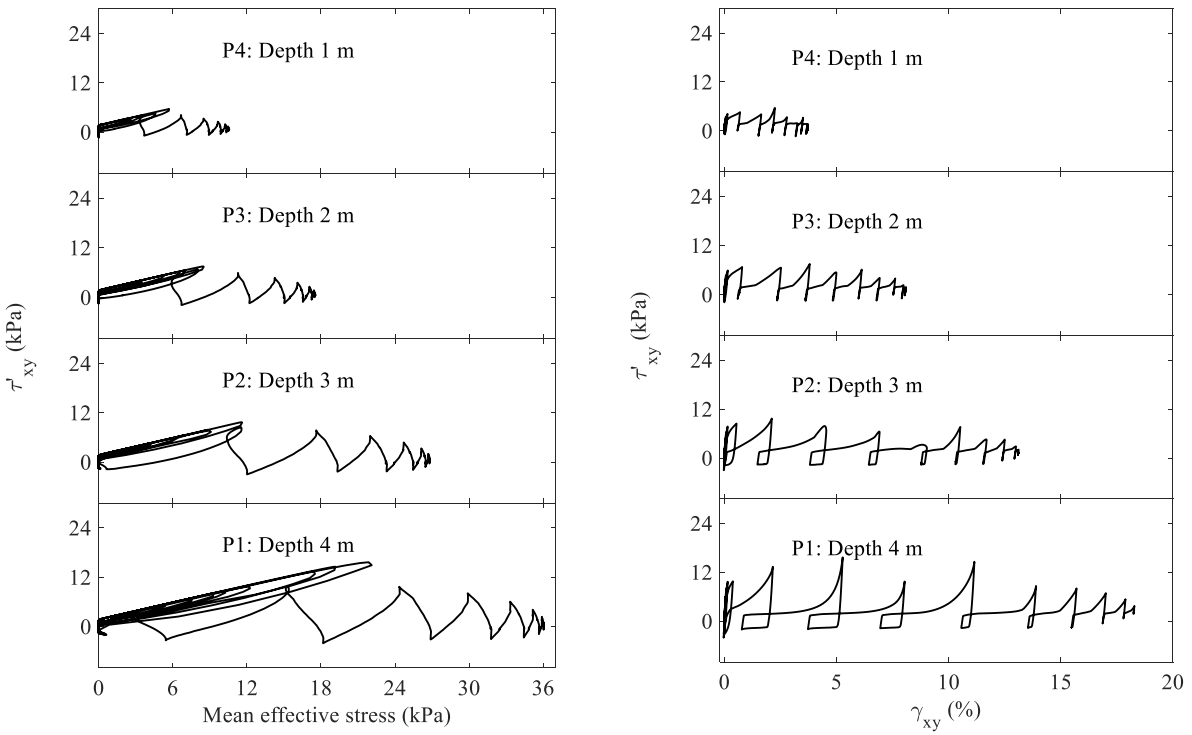

Figure 9. Computed soil responses of RPI-A-B1-1: (a) Mean effective stress-shear stress; (b) Shear stress-strain.

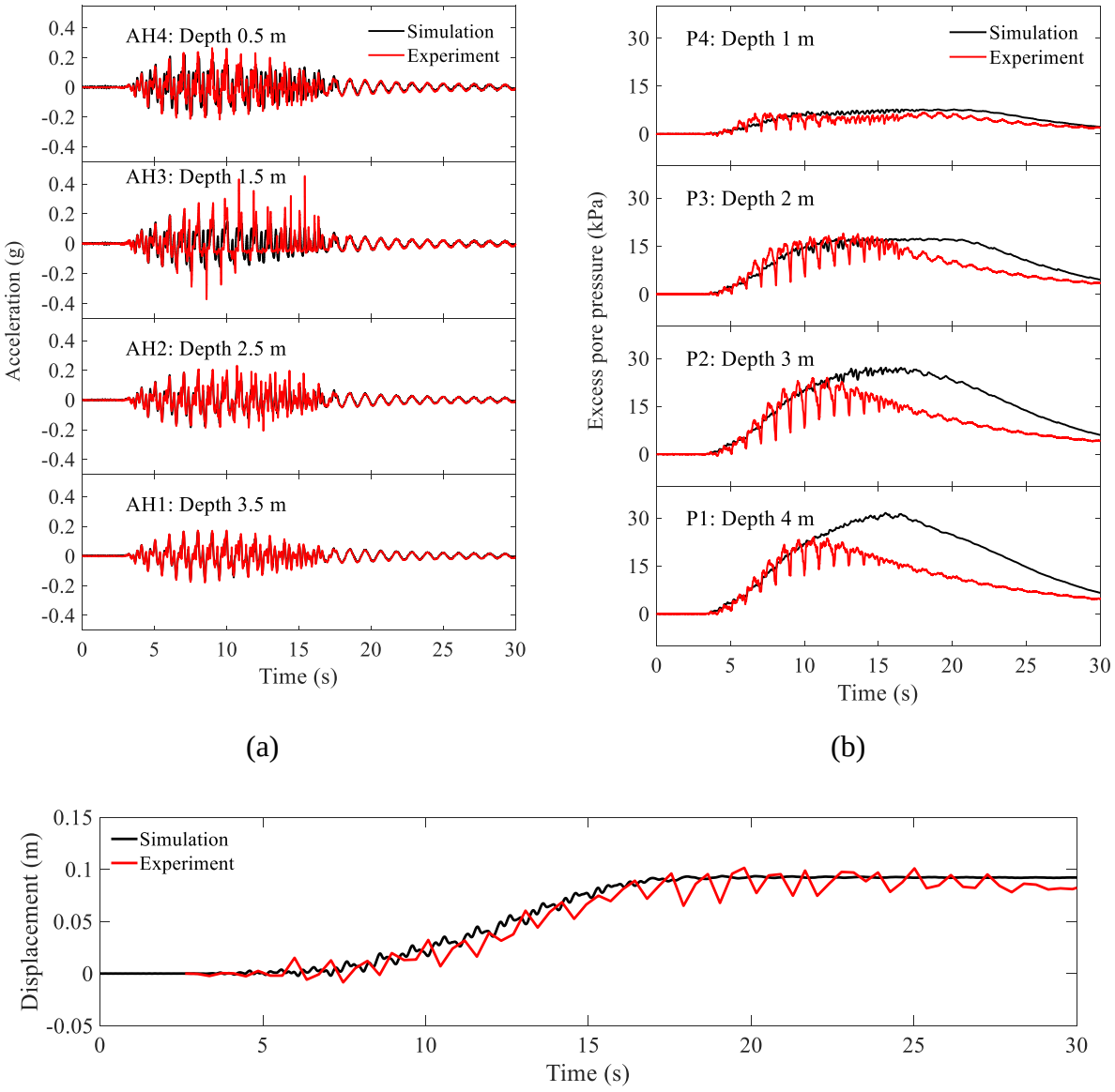

Figure 10. Measured and computed time histories of KyU-A-B2-1: (a) Acceleration; (b) Excess pore water pressure; (c) Displacement at middle of ground surface.

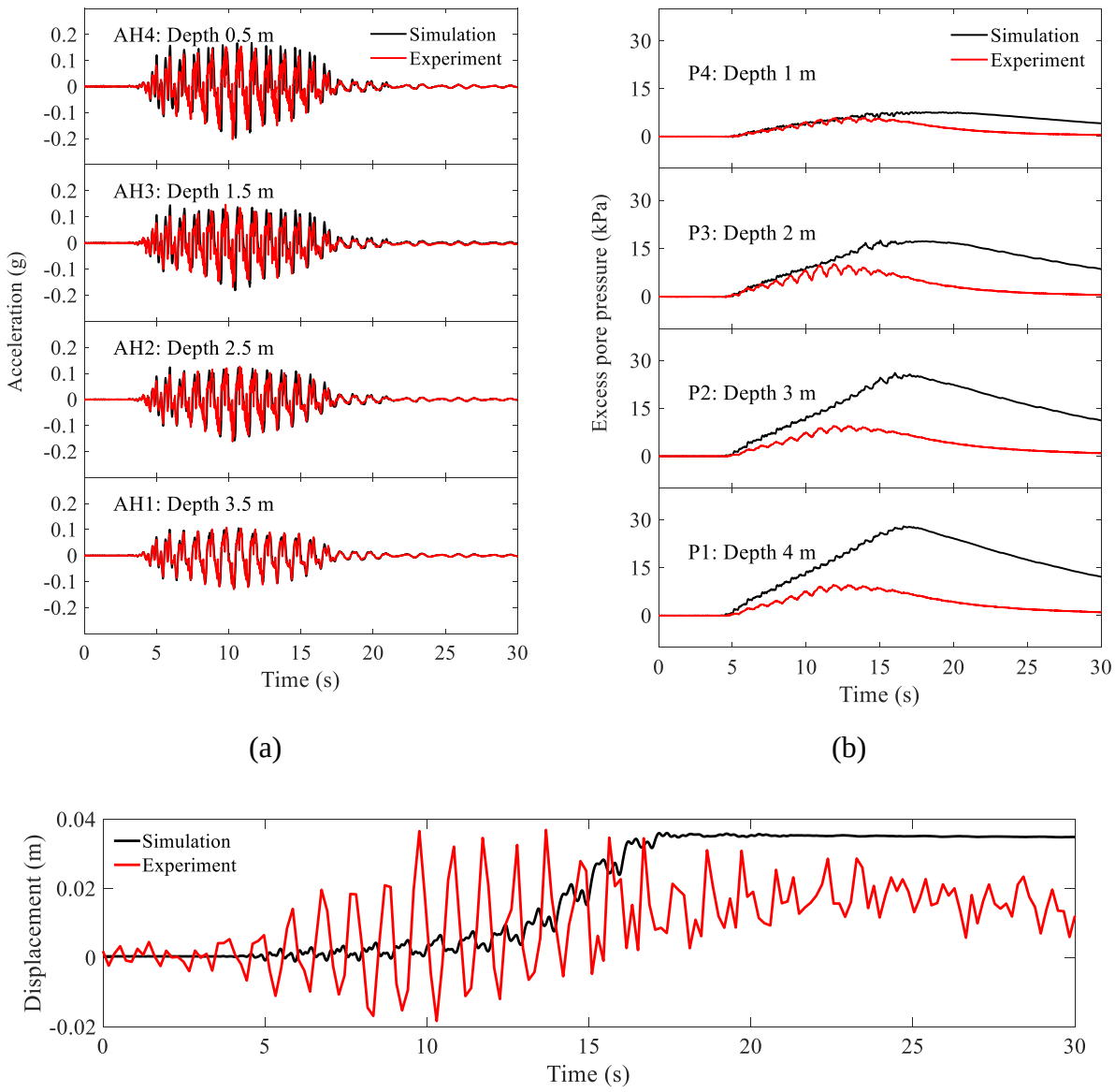

Figure 11. Measured and computed time histories of KyU-A-A2-1: (a) Acceleration; (b) Excess pore water pressure; (c) Displacement at middle of ground surface.

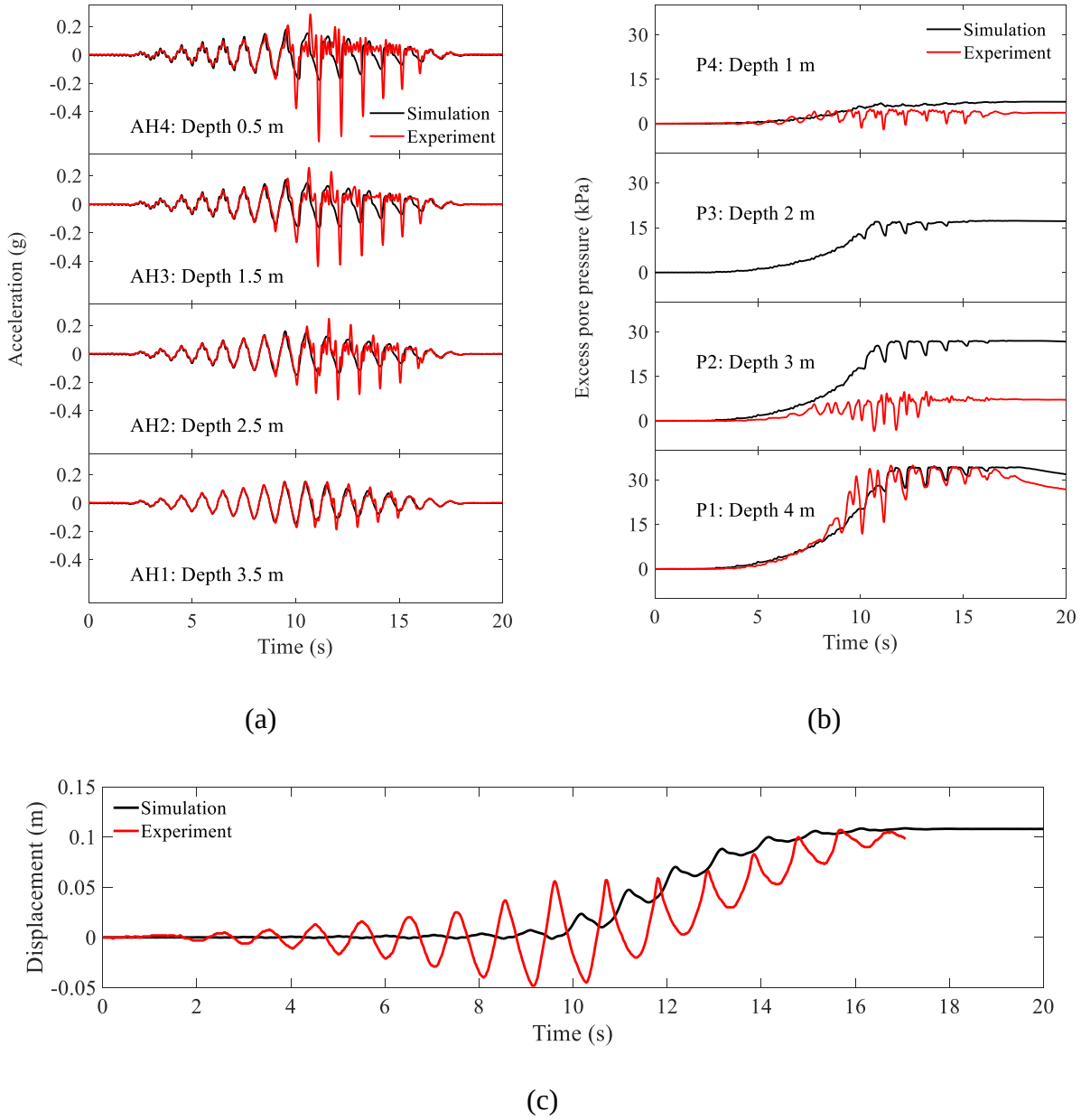

Figure 12. Measured and computed time histories of RPI-A-A1-1: (a) Acceleration; (b) Excess pore water pressure; (c) Displacement at middle of ground surface.

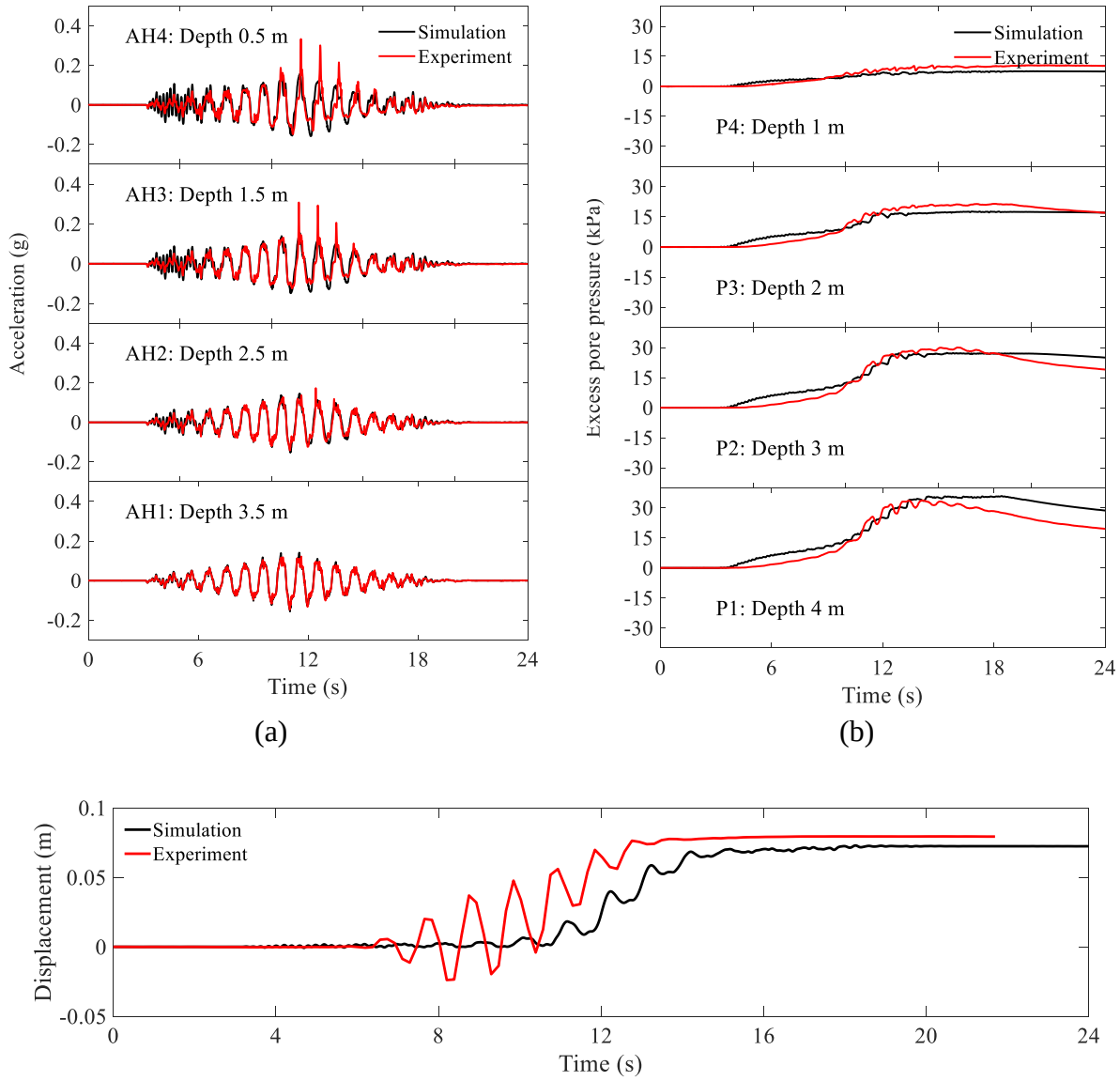

Figure 13. Measured and computed time histories of UCD-A-A2-1: (a) Acceleration; (b) Excess pore water pressure; (c) Displacement at middle of ground surface.

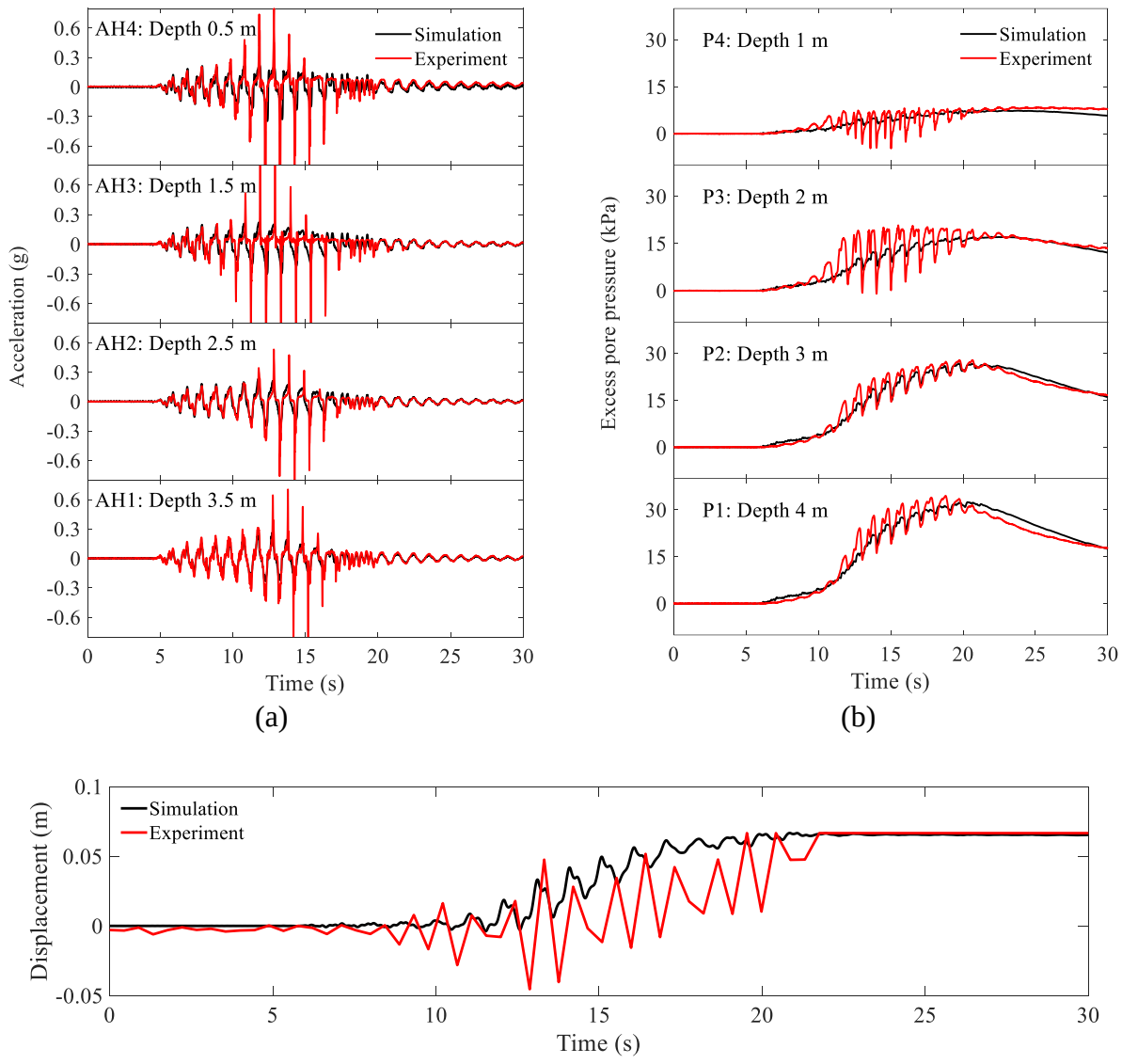

Figure 14. Measured and computed time histories of KyU-A-A1-1: (a) Acceleration; (b) Excess pore water pressure; (c) Displacement at middle of ground surface.

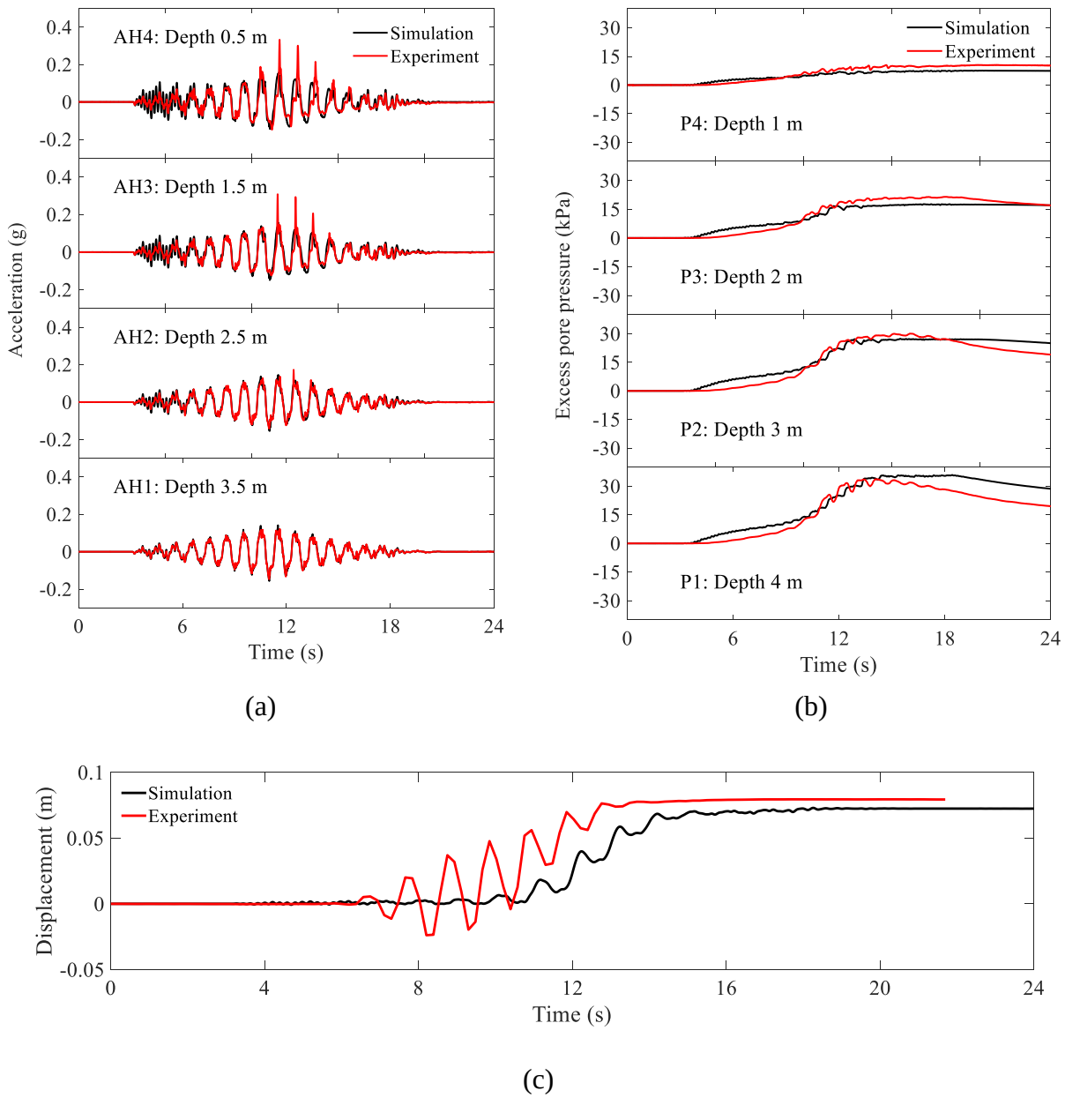

Figure 15. Measured and computed time histories of UCD-A-A1-1: (a) Acceleration; (b) Excess pore water pressure; (c) Displacement at middle of ground surface.

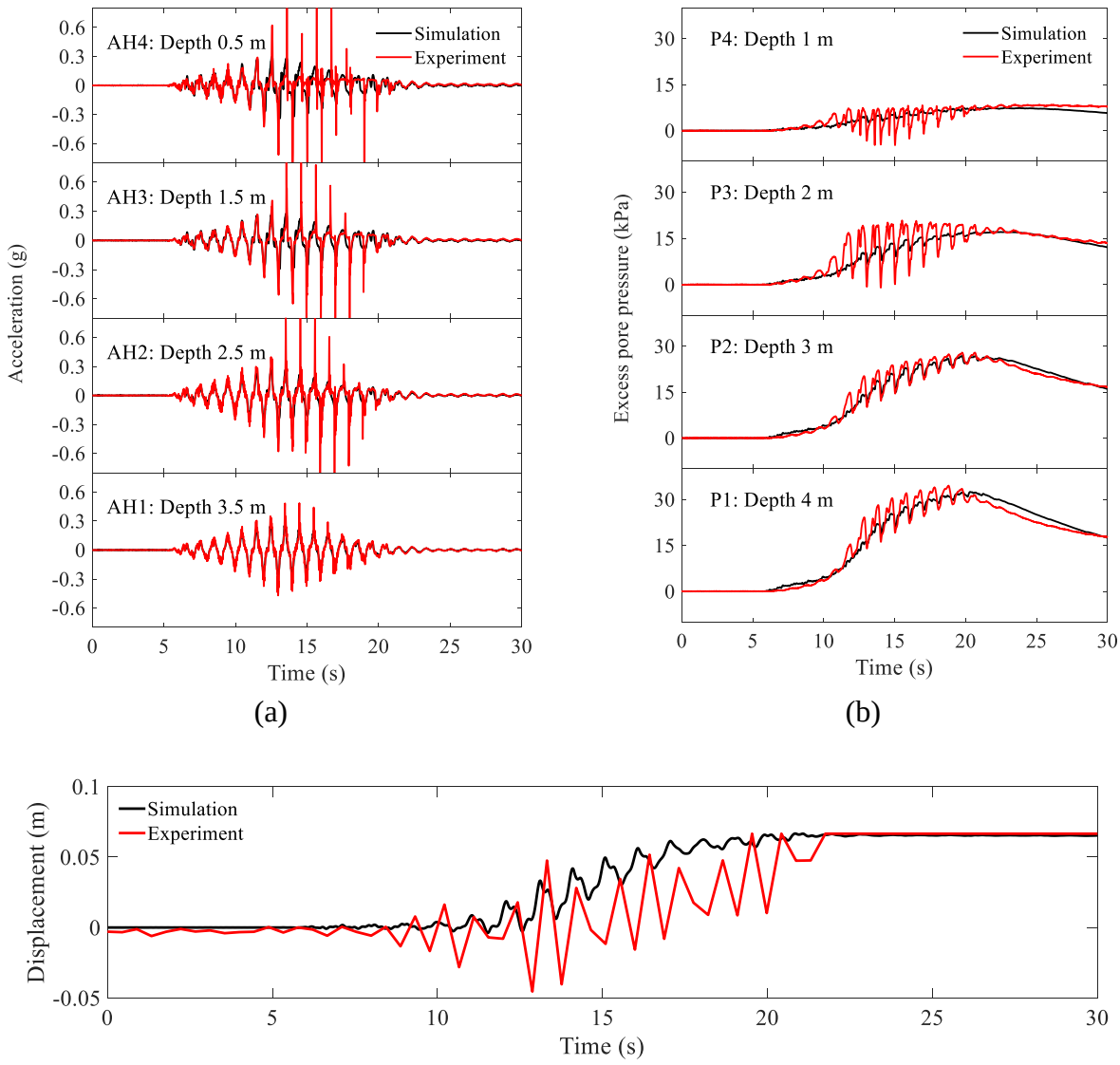

Figure 16. Measured and computed time histories of KyU-A-B1-1: (a) Acceleration; (b) Excess pore water pressure; (c) Displacement at middle of ground surface.

References

Armstrong, R.J., (2017). "Numerical analysis of LEAP centrifuge tests using a practice-based approach." *Soil Dynamics and Earthquake Engineering*.

Arduino, P., Ashford, S., Assimaki, D., Bray, J., Eldridge, T., Frost, D., Hashash, Y., Hutchinson, T., Johnson, L., Kelson, K. and Kayen, R. (2010). "Geo-engineering reconnaissance of the 2010 Maule, Chile earthquake." *GEER Association Report* No. GEER-022, 1.

Bastidas, A.M.P., (2016). "Ottawa F-65 Sand Characterization." University of California, Davis.

Berrill, J.B., Christensen, S.A., Keenan, R.P., Okada, W. and Pettinga, J.R., (2001). "Case study of lateral spreading forces on a piled foundation." *Geotechnique*, 51(6): 501-517.

Carlson, N.N. and Miller, K., (1998). "Design and application of a gradient-weighted moving finite element code II: in two dimensions." *SIAM Journal on Scientific Computing*, 19(3): 766-798.

Chan A. H. C. (1988). "A unified finite element solution to static and dynamic problems in geomechanics." *PhD Thesis*, University College of Swansea.

Chen, W.F. and Mizuno, E. (1990). Nonlinear Analysis in Soil Mechanics, Theory and Implementation, Elsevier, New York, NY.

Elgamal A., Yang Z., and Parra E. (2003). "Modeling of cyclic mobility in saturated cohesionless soils." *International Journal of Plasticity*, 19(6): 883-905.

ElGhoraiby, M. A., Park, H., and Manzari, M. T. (2018). "Physical and Mechanical Properties of Ottawa F-65 Sand."

Ghofrani, A. and Arduino, P., (2017). "Prediction of LEAP centrifuge test results using a pressure-dependent bounding surface constitutive model." *Soil Dynamics and Earthquake Engineering*.

Hamada, M., Isoyama, R. and Wakamatsu, K., (1996). "Liquefaction-induced ground displacement and its related damage to lifeline facilities." *Soils and foundations*, 36(Special): 81-97.

Iwan, W. D. (1967). "On a class of models for the yielding behavior of continuous and composite systems." *Journal of Applied Mechanics*, ASME, 34, 612-617.

Khosravifar, A., Elgamal, A., Lu, J. and Li, J., (2018). "A 3D model for earthquake-induced liquefaction triggering and post-liquefaction response." *Soil Dynamics and Earthquake Engineering*, 110: 43-52.

Kutter, B.L., Manzari, M.T., Zeghal, M., Zhou, Y.G. and Armstrong, R.J., (2014). "Proposed outline for LEAP verification and validation processes." *Safety and Reliability: Methodology and Applications,* p.99

Kutter, B.L., Carey, T.J., Hashimoto, T., Manzari, M.T., Vasko, A., Zeghal, M. and Armstrong, R.J., (2015), "November. LEAP Databases for Verification, Validation, and Calibration of Codes for Simulation of Liquefaction." *In Sixth International Conference on Earthquake Geotechnical Engineering*, Christchurch, New Zealand.

Kutter, B.L., Carey, T.J., Hashimoto, T., Zeghal, M., Abdoun, T., Kokkali, P., Madabhushi, G., Haigh, S.K., d'Arezzo, F.B., Madabhushi, S. and Hung, W.Y., (2017). "LEAP-GWU-2015 experiment specifications, results, and comparisons." *Soil Dynamics and Earthquake Engineering*.

Lacy, S. (1986). "Numerical Procedures for Nonlinear Transient Analysis of Two-phase Soil System." *Ph.D. dissertation*, Princeton University, New Jersey.

Ledezma, C., & Bray, J. D. (2010). "Probabilistic performance-based procedure to evaluate pile foundations at sites with liquefaction-induced lateral displacement." *Journal of geotechnical and geoenvironmental engineering*, 136(3): 464-476.

Manzari, M.T., Kutter, B.L., Zeghal, M., Iai, S., Tobita, T., Madabhushi, S.P.G., Haigh, S.K., Mejia, L., Gutierrez, D.A., Armstrong, R.J. and Sharp, M.K., (2014). "September. LEAP projects: concept and challenges." *In n Proceedings, 4th International Conference on Geotechnical Engineering for Disaster Mitigation and Rehabilitation*, p. 109-116.

Manzari, M.T., El Ghoraiby, M., Kutter, B.L., Zeghal, M., Abdoun, T., Arduino, P., Armstrong, R.J., Beaty, M., Carey, T., Chen, Y. and Ghofrani, A., (2017). "Liquefaction experiment and analysis projects (LEAP): Summary of observations from the planning phase." *Soil Dynamics and Earthquake Engineering*.

Mazzoni, S., McKenna, F., Scott, M. H., and Fenves, G. L., (2009). "Open System for Earthquake Engineering Simulation, User Command-Language Manual." Pacific Earthquake Engineering Research Center, University of California, Berkeley, OpenSees version 2.0, May.

McKenna, F., Scott, M. H., and Fenves, G. L., (2010). "Nonlinear finite-element analysis software architecture using object composition." *Journal of Computing in Civil Engineering*, 24(1): 95–107.

Mroz, Z. (1967). "On the description of anisotropic work hardening." *Journal of the Mechanics and Physics of Solids*, 15(3): 163-175.

Parra E. (1996). "Numerical modeling of liquefaction and lateral ground deformation including cyclic mobility and dilation response in soil systems." *PhD Thesis*. Rensselaer Polytechnic Institute.

Prevost J. H. (1978). "Plasticity theory for soil stress-strain behavior." *Journal of the Engineering Mechanics Division*, 104(5): 1177-1194.

Prevost J. H. (1985). "A simple plasticity theory for frictional cohesionless soils." *Soil Dynamics and Earthquake Engineering*, 4(1): 9-17.

Ueda, K. and Iai, S., (2016). "Numerical Predictions for Centrifuge Model Tests of a Liquefiable Sloping Ground Using a Strain Space Multiple Mechanism Model Based on the Finite Strain Theory." *Soil Dynamics and Earthquake Engineering*.

Vasko, A., (2015). "An Investigation into the Behavior of Ottawa Sand through Monotonic and Cyclic Shear Tests." The George Washington University.

Verdugo, R., Sitar, N., Frost, J.D., Bray, J.D., Candia, G., Eldridge, T., Hashash, Y., Olson, S.M. and Urzua, A. (2012) "Seismic performance of earth structures during the February 2010 Maule, Chile, earthquake: dams, levees, tailings dams, and retaining walls." *Earthquake Spectra*, 28(S1): S75-S96.

Wotherspoon, L., Bradshaw, A., Green, R., Wood, C., Palermo, A., Cubrinovski, M. and Bradley, B., (2011). "Performance of bridges during the 2010 Darfield and 2011 Christchurch earthquakes." *Seismological Research Letters*, 82(6): 950-964.

Yang Z. (2000). "Numerical modeling of earthquake site response including dilation and liquefaction." *PhD Thesis*, Columbia University.

Yang Z., and Elgamal A. (2002). "Influence of permeability on liquefaction-induced shear deformation." *Journal of Engineering Mechanics*, 128(7): 720-729.

Yang Z., Lu J., and Elgamal A. (2008). "OpenSees soil models and solid-fluid fully coupled elements user manual." University of California, San Diego, La Jolla, CA.

Youd, T.L., (1993). Liquefaction-induced damage to bridges. *Transportation Research Record*, 1411, p.35-41.

Zeghal, M., Goswami, N., Kutter, B.L., Manzari, M.T., Abdoun, T., Arduino, P., Armstrong, R., Beaty, M., Chen, Y.M., Ghofrani, A. and Haigh, S., (2017). "Stress-strain response of the LEAP-2015 centrifuge tests and numerical predictions." *Soil Dynamics and Earthquake Engineering*.

Zienkiewicz O. C., Chan A. H. C., and Pastor M. (1990). “Static and dynamic behavior of soils: a rational approach to quantitative solutions. I. fully saturated problems.” *Proceedings of the Royal Society London, Series A, Mathematical and Physical Sciences*, 429(1877): 285-309.

Ziotopoulou, K., (2017). “Seismic response of liquefiable sloping ground: Class A and C numerical predictions of centrifuge model responses.” *Soil Dynamics and Earthquake Engineering*.